Applied and Environmental Microbiology, July 2009, p. 4391–4397 Vol. 75, No. 13
0099-2240/09/$08.00+0 doi:10.1128/AEM.01567-08

CO_2 Production as an Indicator of Biofilm Metabolism▽†

Otini Kroukamp and Gideon M. Wolfaardt*

Department of Chemistry and Biology, Ryerson University, 350 Victoria Street, Toronto, Ontario M5B 2K3, Canada

Received 9 July 2008/Accepted 30 March 2009

Biofilms are important in aquatic nutrient cycling and microbial proliferation. In these structures, nutrients like carbon are channeled into the production of extracellular polymeric substances or cell division; both are vital for microbial survival and propagation. The aim of this study was to assess carbon channeling into cellular or noncellular fractions in biofilms. Growing in tubular reactors, biofilms of our model strain *Pseudomonas* sp. strain CT07 produced cells to the planktonic phase from the early stages of biofilm development, reaching pseudo steady state with a consistent yield of $\sim 10^7$ cells $\cdot$ cm^{-2} $\cdot$ h^{-1} within 72 h. Total direct counts and image analysis showed that most of the converted carbon occurred in the noncellular fraction, with the released and sessile cells accounting for <10% and <2% of inflowing carbon, respectively. A CO_2 evolution measurement system (CEMS) that monitored CO_2 in the gas phase was developed to perform a complete carbon balance across the biofilm. The measurement system was able to determine whole-biofilm CO_2 production rates in real time and showed that gaseous CO_2 production accounted for 25% of inflowing carbon. In addition, the CEMS made it possible to measure biofilm response to changing environmental conditions; changes in temperature or inflowing carbon concentration were followed by a rapid response in biofilm metabolism and the establishment of new steady-state conditions.

Notable advances have been made in the study of biofilms since the early recognition (for examples, see references 11 and 29) of this form of microbial existence. Following these earlier studies of selective adherence of bacteria to surfaces was the development of continuous flow cells, as well as computer-assisted and scanning confocal laser microscopy that enabled the improved description of bacterial behavior at surfaces (for an example, see reference 23), and we now know that biofilms are organized aggregates of extracellular polymeric substance (EPS)-enclosed cells that differ substantially from suspended cells (47). Observing biofilm phenotypic responses may provide insight to guide researchers in conducting directed experiments to unravel underlying fundamental mechanisms; however, we still lack methods to measure and monitor biofilm function.

Flemming (9) grouped industrial biofilm monitoring systems into the following three categories: (i) systems detecting the increase and decrease of materials accumulating on a surface without differentiating biomass from other components, (ii) those that can distinguish between biotic and abiotic material, and (iii) those that provide detailed chemical information of biofilms. Janknecht and Melo (16) categorized online biofilm monitoring techniques in a similar way when comparing applications in industrial systems but added a category for monitoring metabolic activity (a category that Flemming [9] hinted at with the proposal of a technique that can distinguish between living and dead organisms on a surface).

In brief, a nonexhaustive list of techniques that deal only with online monitoring increase (whether of biotic or abiotic origin) and the decrease of biofilms includes quartz crystal microbalances (48), large area photometry (3, 33), electrical capacitance (31), fiber optical devices (49), differential turbidity measurement devices (20), microfluidic biochips (39), optical coherence tomography (13), pressure drop or friction resistance (24), and heat transfer resistance (28). Techniques that provide information about the physical structure and chemical properties of biofilms are nuclear magnetic resonance (44), attenuated total reflectance-Fourier transform infrared spectroscopy (7), and photoacoustic spectroscopy (43). Some biofilm monitoring techniques provide information about metabolic activity in biofilms, such as those using electrochemical devices like dissolved oxygen and redox probes (25), microbiologically influenced corrosion monitoring (34), nuclear magnetic resonance (56), measurement of substrate consumption (19, 50) or metabolic products (53), bioluminescence assays, and fluorometry (56).

The objective of the study was to develop a real-time monitoring system to measure gaseous CO_2 production as an indicator of biofilm metabolism and to use the system to determine the biofilm response to environmental conditions and to measure carbon channeling in biofilms.

MATERIALS AND METHODS

Culture media and growth conditions. Pure culture biofilms of *Pseudomonas* sp. strain CT07 *gfp* (3) and *Pseudomonas aeruginosa* PA01 *gfp* were grown in silicone tubes (42). The silicone tubes were inoculated with 200 to 500 μl from an overnight culture (the same medium was used as that described below except 5 mM of sodium citrate was used instead of 1 mM) with the pump turned off for 30 min to 1 h to allow initial adhesion to the tube walls. Sterile defined growth medium [a final concentration of 1.51 mM $(NH_4)_2SO_4$, 3.37 mM Na_2HPO_4, 2.20 mM KH_2PO_4, 179 mM NaCl, 0.1 mM $MgCl_2 \cdot 6H_2O$, 0.01 mM $CaCl_2 \cdot 2H_2O$, 0.001 mM $FeCl_3$] with either 1 mM sodium citrate or 3 mM glucose as the sole carbon source was continuously supplied by a Watson Marlow 205U peristaltic pump at 15 ml/h (unless specified otherwise). Medium retention time was 12 min for this reactor size and flow rate.

CEMS and measurements. A carbon dioxide evolution measurement system (CEMS) was constructed, which is essentially a silicone tube biofilm reactor

* Corresponding author. Mailing address: Department of Chemistry and Biology, Ryerson University, 350 Victoria Street, Toronto, ON M5B 2K3, Canada. Phone: (416) 979-5000, ext. 4051. Fax: (416) 979-5044. E-mail: gwolfaar@ryerson.ca.

† Supplemental material for this article may be found at http://aem.asm.org/.

▽ Published ahead of print on 3 April 2009.

(inside diameter, 0.16 cm; outside diameter, 0.24 cm; length, 150 cm; VWR International, Mississauga, ON, Canada) encased in a sealed Tygon tube (inside diameter, 0.48 cm; outside diameter, 0.79 cm; formulation R-3603; VWR International, Mississauga, ON, Canada) with the annular space being connected to a CO_2 analyzer. Silicone tubing has a relatively high permeability to both CO_2 and O_2 compared to that of Tygon tubing; approximately 50 times and 200 times higher for CO_2 and O_2, respectively, according to permeability coefficients provided by the manufacturer. Given a higher gaseous CO_2 concentration on the inside of the lumen of the silicone tube due to biofilm metabolic activity, it can be assumed that a fraction will cross the silicone tube wall to the annular space where it can be measured. The annular space of the carbon dioxide exchange system (CEMS) was connected to an absolute, nondispersive, infrared LI-820 CO_2 gas analyzer (LI-COR Biosciences, NE), and compressed air was used as the sweeper gas. The steady-state CO_2 concentration in the compressed air was measured and subtracted from the steady-state CO_2 originating from the CEMS. Gas flow rates were determined by volumetric displacement and a thermal gas mass flow meter (Aalborg, NY).

Although the use of silicone for carbon dioxide transfer has been applied to measure microbial metabolic activity in water research and fermentations, such an approach has to our knowledge not been applied in biofilm studies. For example, Visser et al. (54) and Aboka et al. (1) measured the transfer of O_2 and CO_2 across silicone membranes to monitor respiration of *Saccharomyces cerevisiae* isolates grown in a chemostat, and Dahod (6) used submerged silicone tubes in a fermentor to measure respiration rates of industrial *Streptomyces* organisms on a pilot plant scale.

Theory. During development of the CEMS, it was clear that it would be useful to have a mathematical relationship that determines what fraction of CO_2 will cross the silicone membrane under certain experimental conditions. In this way, it would be necessary to measure only the CO_2 concentration on one side while being able to relate it to the CO_2 concentration on the other side of the membrane.

Gas transport across silicone membranes. Gas mass transfer across a membrane is often described in terms of Fick's law of diffusion (for examples, see references 36 and 15) as follows:

$$J = -D\frac{dc}{dx} = \frac{D}{\Delta l}(c_{m1} - c_{m2}) \quad (1)$$

where c describes the concentrations (mol · m^{-3}), x is the length (m), J is the flux of the compound crossing the membrane (mol · s^{-1} · m^{-2}), D is the diffusion coefficient (m^2 · s^{-1}), Δl is the thickness of the membrane, and c_{m1} and c_{m2} (mol · m^{-3}) are the concentrations of the species crossing the membrane at the membrane surfaces on either side.

Silicone membranes can be described as nonporous (dense-polymer) membranes like the kind used for pervaporation, perstraction, or gas separations as opposed to porous membranes used in microfiltration or ultrafiltration (36).

In addition to diffusion, the partitioning of the solute between the membrane and adjacent solution plays an important role in the transport. The partitioning of solute between the adjacent solution and the membrane surface is linearly related via a partitioning coefficient analogous to a Henry's law constant of the form $\sigma_1 = c_m(\text{eq})/C_1^{\text{in}}(\text{eq})$ and $\sigma_2 = c_m(\text{eq})/C_2^{\text{out}}(\text{eq})$, where σ_1 is the partitioning coefficient (sometimes called a solubility coefficient, but it serves the same purpose of relating the surface membrane concentration to the adjacent phase concentration), and C_1^{in} is the solute concentration in the adjacent phase in equilibrium (eq) with the solute concentration at the membrane surface (c_m). If the adjacent or bulk solutions are the same (e.g., aqueous), $\sigma_1 = \sigma_2 = \sigma$ and equation 1 can be written as

$$J = \frac{D}{\Delta l}(\sigma C_1^{\text{in}} - \sigma C_2^{\text{out}}) = \frac{\sigma D}{\Delta l}(C_1^{\text{in}} - C_2^{\text{out}}) \quad (2)$$

Note that the partitioning coefficient can be written in many forms, depending on the driving force (partial pressure or concentration difference across the membrane). It can be dimensionless or can relate partial pressure to concentration or vice versa, so attention has to be given to the appropriate units. Under certain conditions with specific membrane polymers and permeants, the permeability coefficient, P, can be given as the product of the diffusion constant, D, and the partitioning coefficient, σ. The partition coefficient serves as an indicator of the ability of the membrane to allow transport of certain molecules. Again, the units of P may vary widely depending on the driving force (58).

Depending on the nature (e.g., the size of the molecule) of the solute and membrane properties, diffusion or solubility of the solute in the membrane (σ) will contribute in different amounts to the overall mass transfer. In the case of carbon dioxide transfer through rubber or silicone, solubility plays by far the most important role in gas transport (36).

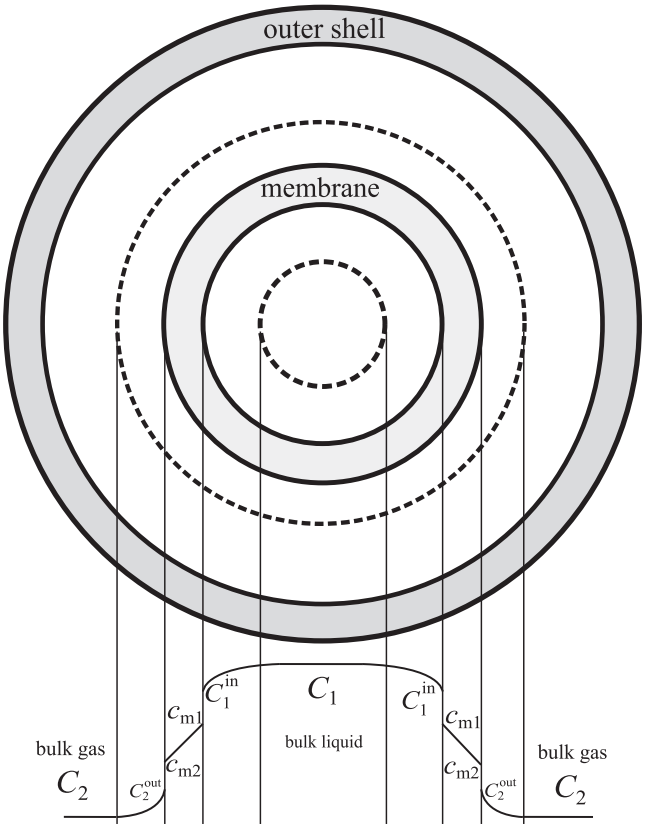

FIG. 1. Cross section to illustrate radial transfer of CO_2 from the liquid bulk phase to the gas bulk phase in the CEMS. Adapted from reference 8 with permission from Elsevier.

Gas transport across a silicone tube wall in the CEMS. The permeability of silicone rubber membranes to O_2 and CO_2 has long been known and is implied in liquid-gas contact applications, such as a membrane gills for submarines and underwater stations (40) or gas exchange in blood (46). However, when the two phases adjacent to the membrane are not the same, equation 2 does not accurately describe the mass transfer anymore. The different phases will pose different mass transfer resistances on either side of the membrane, and the partitioning coefficients may vary (see references 17, 32, and 60 for examples).

If the solutions adjacent to the membrane are not the same (e.g., aqueous and gas) (5), $\sigma_1 \neq \sigma_2$ and equation 1 becomes as follows:

$$J = \frac{D}{\Delta l}(\sigma_1 C_1^{\text{in}} - \sigma_2 C_2^{\text{out}}) \quad (3)$$

The concentrations for C_1^{in} and C_2^{out} are usually not the same as the concentrations in the bulk solutions, C_1 and C_2. For a steady-state flux of solute from bulk solution 1 to bulk solution 2, the fluxes can be expressed as follows: $J = k_1(C_1 - C_1^{\text{in}}) = D/\Delta l(\sigma_1 C_1^{\text{in}} - \sigma_2 C_2^{\text{out}}) = k_2(C_2^{\text{out}} - C_2)$, where k_1 and k_2 are mass transfer coefficients (m · s^{-1}) (45). The relationship described above can be simplified as follows:

$$J = \frac{1}{\frac{\sigma_1}{k_1} + \frac{\Delta l}{D} + \frac{\sigma_2}{k_2}}(\sigma_1 C_1 - \sigma_2 C_2) = \frac{1}{\frac{\sigma_1}{k_1\sigma_2} + \frac{\Delta l}{D\sigma_2} + \frac{1}{k_2}}\left(\frac{\sigma_1}{\sigma_2}C_1 - C_2\right) \quad (4)$$

If the bulk solution on side 1 is water and the bulk solution on side 2 is air, based on equation 4, a local transfer coefficient (K_z) can be written as $1/K_z = \sigma_1/k_1\sigma_2 + \Delta l/D\sigma_2 + 1/k_2$, and equation 4 can be rewritten as follows:

$$J = K_z\left(\frac{\sigma_1}{\sigma_2}C_1 - C_2\right) \quad (5)$$

Equation 5 describes the radial transfer from the liquid bulk phase to the gas bulk phase (Fig. 1). To determine the overall transfer coefficient (K_L) of the CEMS, a mass balance can be written across an infinitely thin slice of the CEMS

and integrated along the length of the tube, similar to treatment carried out by Dindore et al. (8).

The average flux over the entire length of the tube can be shown by the following equation:

$$J_{ave} = \frac{Q_2\left(HC_1 - HC_1 e^{-\frac{\pi d_0 K_L}{Q_2}L}\right)}{\pi L d_0} \quad (6)$$

where J_{ave} is the average flux (mol · m^{-2} · s^{-1}), Q_2 is the volumetric flow rate of the gas (m^3/s), H is a Henry's law constant relating equilibrium values (σ_1/σ_2), L is the length of the tube (m), and d_0 is the outer diameter of the silicone tube (m). Note that in the derivation of equation 6, it is assumed that the concentration on the liquid side remains constant throughout the length of the reactor tube (see the supplemental material). With equation 6, it is therefore possible to determine the overall transfer coefficient for the CEMS, K_L, with known liquid phase CO_2 concentrations (C_1) by measuring the CO_2 flux appearing in the gas phase. Once calibrated for a particular membrane configuration, the gas phase results can be used to calculate the C_1 for other experimental conditions.

In an experimental configuration where microbes grow in a biofilm on the inside wall of the silicone tube, they will excrete their CO_2 into their surroundings. The CO_2 from microbial respiration is transferred across cell membranes in a dissolved form or aqueous CO_2 (18). Aqueous CO_2 can either be converted to a gaseous form or remain dissolved and even be transformed into bicarbonate and carbonate ions as schematically represented by Zeng (59).

$$\begin{array}{ll} CO_2^{\text{measured}} & CO_2^{\text{in vivo}} \\ \uparrow & \downarrow \end{array}$$

$$CO_2(g) \leftrightarrow CO_2(aq) \leftrightarrow H_2CO_3 \leftrightarrow HCO_3^- + H^+ \leftrightarrow CO_3^{2-} + 2H^+ \quad (7)$$

The ratio of the dissolved forms of CO_2 is dependent on pH, temperature, and ion activity (10). At a pH of 4 to 7, the carbonate ion concentration is negligible.

Linearity of dissolved carbon dioxide. A dilution series of dissolved CO_2 was used to correlate the amount of CO_2 in the liquid phase transferred by the CEMS to the gas phase. A saturated solution of CO_2 in Milli-Q water was made by stirring pieces of "dry ice" (solid CO_2) until the pH stabilized at room temperature. This saturated solution was used to make a dilution series of 1% to 4% (vol/vol) dissolved CO_2 and sealed in serum vials with butyl rubber stoppers. Steady-state CO_2 concentrations in the off-gas were measured with increasingly dissolved CO_2 samples.

Effect of temperature on biofilm respiration/metabolism. To test the sensitivity of biofilm respiration to temperature changes, the CEMS was submerged in a cooling water bath overnight at 15°C and subsequently subjected to changes in temperature between 27°C and 10°C and CO_2 concentrations in the off-gas measured. To ensure an even distribution of temperature, the carrier gas and growth medium were controlled in the same water bath as the CEMS.

Effect of citrate or glucose concentration. In each replicate experiment, biofilms were grown for 8 days in the CEMS at citrate and glucose concentrations of 1 mM and 3 mM, respectively, at room temperature before the influent concentrations were randomly varied between 0.125 mM and 5 mM and the CO_2 concentrations were measured in the off-gas. The validity of the biofilm response to different citrate or glucose concentrations in a carbon-limited environment was tested with the following relationship described by Gillooly et al. (12): metabolic rate $\propto$ (concentration of reactants)(fluxes of reactants)(kinetic energy of the system). For the conditions where only the concentrations of the carbon source were varied, the last two terms can be considered constant.

Determination of cell numbers and carbon in cellular and noncellular fractions. Cell numbers in the effluent and biofilm were determined by heterotrophic plate counts and total direct cell counts. In brief, cell suspensions were vortexed and diluted in 0.9% saline and stained with 4′,6-diamidino-2-phenylindole (DAPI). The suspension was filtered onto a 0.22-μm black polycarbonate filter, and the cell numbers were determined by epifluorescence microscopy. Images were recorded with a Leica DM5000 B epifluorescence microscope and a Leica DFC350 FX camera, and cell sizes were determined on a PC computer using the Microsoft Windows version of the public domain NIH Image program from the U.S. National Institutes of Health (available at http://rsb.info.nih.gov/nih-image/). Digital image processing was done as described by Massana et al. (30), which involved the application of a series of Gauss, Laplace, and median filters with manual thresholding steps in between. Both cell numbers and cell dimensions could be determined from the processed images. The pseudomonad cells were rod shaped, and cellular volumes were determined by using the following equation: $V = [w^2(\pi/4)](l - w) + [w^3(\pi/6)]$, where w and l are the width and length of the cell, respectively. Values for w and l were determined from the digitally processed images, and the average two-dimensional cell area determined by the equation $[(l - w) \times w + \pi(w/2)^2]$ was 0.98 ± 0.12 μm^2, which is very similar to values of 0.86 ± 0.12 μm^2 for *Pseudomonas fluorescens* as determined by Mueller (35). *Pseudomonas* sp. strain CT07 is closely related to *P. fluorescens* (3).

Posch et al. (38) described an allometric conversion formula to relate cellular volume to cellular carbon based on images obtained for a specific dye. For DAPI-stained images, the conversion is given by the following equation: cellular carbon = $218 \times V^{0.86}$, with the cellular carbon measured in femtograms of carbon and V in micrometers cubed.

Determination of unused citrate exiting the reactor in the liquid phase. Unused citrate exiting the reactor was determined with an enzymatic analysis kit from Enzytec (Scil Diagnostics GmbH, Germany).

Carbon balance. For the carbon balance, both effluent liquid samples and off-gas samples were taken at 24-h intervals and measured for carbon content. These discrete concentration values were used together with the flow rates to calculate the cumulative carbon exiting the CEMS. The total carbon in the effluent was measured with a catalytic combustion, nondispersive infrared total carbon analyzer (TOC-$V_{CSH/CSN}$; Shimadzu, Kyoto, Japan), while the CO_2 in the off-gas was measured as mentioned above. At the end of the experiment, the organic matter that accumulated in the reactor tube was collected by squeezing out the attached organic matter using a bottle as a rolling pin.

Visual observations revealed that as the biofilms matured, small aggregates would sporadically exit the tube reactor with the effluent. These aggregates are denser than water. Therefore a simple trap consisting of a 1.5-ml Eppendorf tube with the influent line positioned below the effluent line was devised for collecting the aggregate-free liquid phase in a container with sodium azide (final concentration, ~70 mg/liter) to inhibit further microbial degradation of carbonaceous compounds.

RESULTS

The CEMS was developed for measuring real-time, whole-biofilm CO_2 production rates. This device was used to assess the biofilm response to changing environmental conditions and carbon channeling in biofilms.

Calibration. When the CEMS was tested with gas phases on both sides of the silicone membrane according to methods described by ASTM standards (2), the gas permeability coefficient was $(3.02 \pm 0.04) \times 10^{-6}$ $cm^3 \cdot mm \cdot s^{-1} \cdot cm^{-2} \cdot cm\ Hg^{-1}$ and corresponded well with values from the manufacturer (same order of magnitude).

Milli-Q water with known dissolved CO_2 concentrations (between 0 and 4% saturation) was used to test the CO_2 transfer across the silicone tube wall to the gas phase. The CO_2 measured in the gas phase was highly linear ($R^2 = 0.999$) with various dissolved CO_2 concentrations.

Experimental results for biofilm CO_2 production were well within the range tested during the calibration experiments.

Effect of temperature on biofilm metabolism. Figure 2 shows an actual output from the CO_2 analyzer. Popular models for describing the dependence of microbial metabolic activity to temperature were used to verify the relationship of steady-state, gaseous CO_2 measurements to variations in temperature. The Arrhenius equation is an exponential function used to model temperature relationships, and the plot of the log of activity (CO_2 measurement) against the inverse of the absolute temperature should be a straight line if the activation energy is constant over the range of measurement (37). Indeed, the results showed an R^2 value equal to 0.990 and 0.977 for growth on 1 mM citrate and 3 mM glucose, respectively, for *Pseudomonas* sp. strain CT07 *gfp*. Another model for relating temperature to microbial activity is a square root relationship used for microbes growing at suboptimal temperatures, which was

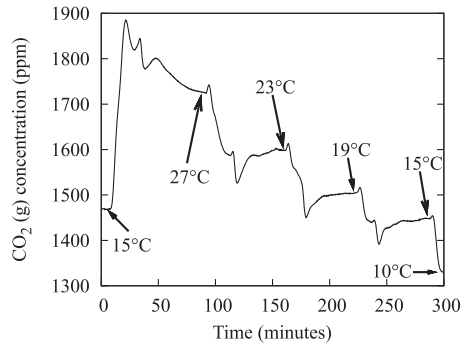

FIG. 2. Effect of temperature on biofilm metabolism. Output data from the CO_2 analyzer showing the response of a *Pseudomonas* sp. strain CT07 *gfp* biofilm and the time to reach new steady-state values with temperature perturbations.

the case for the strains used in these experiments. A plot of the square root of the activity against the temperature should give a straight line (37), which was the case with an R^2 value of 0.988 for growth on 1 mM citrate and an R^2 value of 0.993 for growth on 3 mM glucose for *Pseudomonas* sp. strain CT07 *gfp*.

Duplicate experiments provided similar results in terms of both CO_2 measurements and times to reach steady state (results not shown).

Effect of citrate concentration on biofilm metabolism. The citrate concentrations in the medium were varied at random (Fig. 3B) while measuring the CO_2 in the off-gas. For citrate concentrations between 0.5 mM and 5 mM, the response in CO_2 evolution was nearly linear ($R^2 = 0.996$) for *Pseudomonas* sp. strain CT07 *gfp*. Similarly, the response in CO_2 evolution for *P. aeruginosa* PA01 between 0.5 and 4 mM citrate was also nearly linear, with an R^2 value of 0.995. Because of its wider range of carbon sources, *P. aeruginosa* PA01 was also cultivated on glucose, benzoate, and tryptic soy broth with similar linear responses (R^2 values of 0.996, 0.994, and 0.999, respectively). This metabolic response with various carbon concentrations above the threshold of 0.5 mM (0.3 g/liter in the case of tryptic soy broth) can be explained with the relationship described by Gillooly et al. (12), presented in Materials and Methods. The last two terms in their equation can be considered constant (reasons mentioned below), which leaves the metabolic rate directly proportional to the concentration of reactants (citrate). Microbes have the ability to modulate nutrient uptake and enzyme affinities to ensure high metabolic fluxes even under low-nutrient conditions (with the assumption that fluxes will be kept fairly constant under the conditions of our experiments; i.e., second term) (51). The kinetic energy (third term) of the system is dependent on temperature, which was kept constant during the experiment.

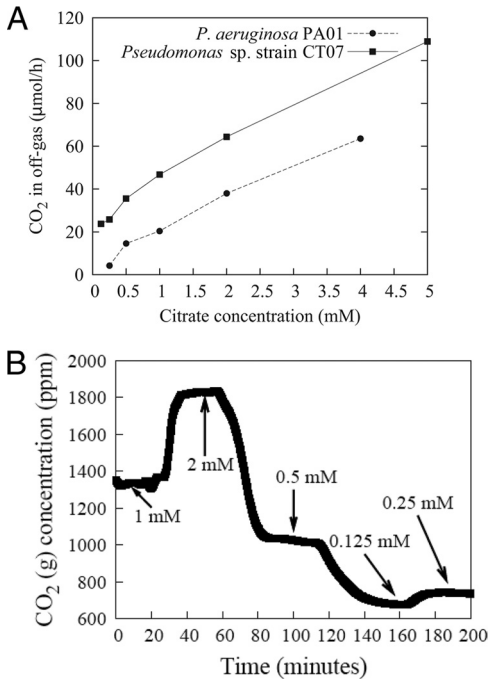

FIG. 3. CO_2 production rates showing biofilm response to changes in influent citrate concentrations. Biofilm metabolic response showing the linear correlation (an R^2 value of 0.995 and 0.996 for *P. aeruginosa* PAO1 and *Pseudomonas* sp. strain CT07, respectively) (A) with citrate concentration despite the random order (*Pseudomonas* sp. strain CT07 in this case) (B) in which the concentration was changed, demonstrating the adaptability of biofilms to environmental changes.

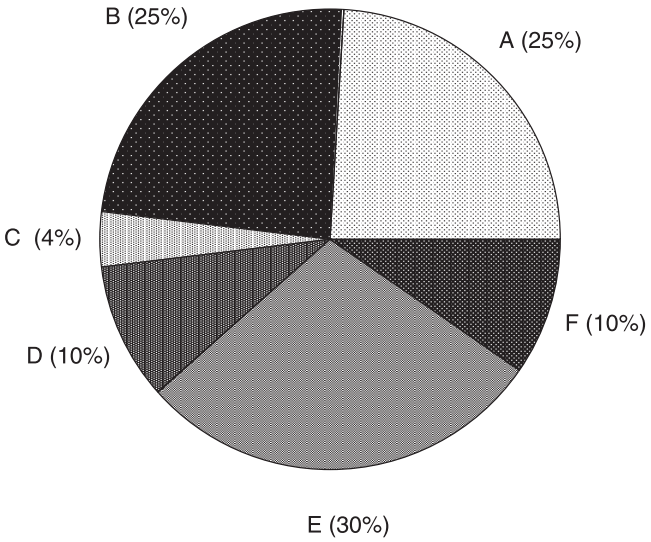

FIG. 4. Carbon balance for a *Pseudomonas* sp. strain CT07 biofilm over an 8-day cultivation. Shown are cumulative CO_2 exiting in gas phase (A), cumulative CO_2 exiting in liquid phase (B), carbon remaining behind in the biofilm (C), cumulative carbon exiting as cells (D), cumulative carbon exiting as aggregates (less than 1% of vol) (E), and cumulative unused citrate (F). The carbon balance typically closed within 2 to 4%.

Carbon balance. All the carbon exiting the biofilm reactor in the liquid (as suspended materials) and gas phases was compared with the carbon flowing into the reactor over a period of 8 days (Fig. 4). The carbon balance for replicate experiments closed to within 2 and 4%. For the experiment summarized in Fig. 4, carbon that exited the reactor in the liquid phase accounted for 72.4% of the incoming carbon. The cumulative amount of gaseous CO_2 leaving the reactor was 24.9% of the inflowing carbon, while 4.1% of the carbon remained attached to the inner surface of the reactor tube. Components that contributed to the liquid phase carbon fraction that exited the

reactor included dissolved CO_2, cellular carbon (biofilm biomass lost, e.g., sloughing, dispersion, and erosion), unused citrate, and EPS. Calibration experiments using known concentrations of dissolved CO_2 and concomitant gas phase measurements showed that at least an amount similar to that of the CO_2 in the gas phase exited the reactor in a dissolved form. Microbial cells in the effluent reached values of $\sim 10^6$ cells $\cdot$ cm^{-2} $\cdot$ h^{-1} (cells produced per biofilm footprint area per unit of time) within 24 h after inoculation and reached pseudo-steady-state values of $\sim 10^7$ cells $\cdot$ cm^{-2} $\cdot$ h^{-1} after 3 days. The C fraction leaving the reactor as nonaggregated cells was always less than 10%, as determined by direct microscopy, image analysis, and the conversion formula described in Materials and Methods. Carbon leaving the reactor as aggregates accounted for 30% of the inflowing carbon condensed in less than 1% of the exiting volume. The composition of these aggregates in terms of cell numbers and other contributing constituents has not yet been determined. Unused citrate plateaued at 10% of the growth medium value after 3 days.

DISCUSSION

Lewandowski and Beyenal (26) lamented the divide between the generation of monitoring results and the useful application thereof, due mainly to the inability of mathematical models to accept the monitored parameters even if the monitoring is done with technical excellence. Building the bridge between biofilm monitoring and mathematical models that can successfully implement the data to correlate measured parameters to biofilm function is beyond the scope of this article. However, we hope to demonstrate that simple biofilm monitoring measurements can provide insight into the important biofilm functions of protection (EPS production) and proliferation (releasing progeny into the environment by physiological means and by employing physical means such as erosion, abrasion, and sloughing). Being aware of the phenomenological responses of biofilms may lead to the identification of focus areas for more fundamental research.

Kreft (21) considered the conflict in biofilms for the economical use of limiting resources to channel it toward either a specific growth rate (the rate of biomass increase per time and biomass) or growth yield (biomass formed per amount of resource used), where a high growth yield can be attained only through a decrease in the specific growth rate. In pure culture work, Bester et al. (3) showed that microbes in a biofilm released high numbers of cells into the environment, even at very early stages of biofilm development. EPS production varies with different physical environmental conditions and available nutrients. Xavier et al. (57) simulated competition between microbial strains that differ in their ability to produce EPS. They concluded that polymer production may afford a competitive advantage in mixed-species biofilms under certain conditions by suffocating neighboring nonpolymer producers and exposing later generations to better oxygen conditions. CO_2 production is another important and often neglected sink of carbon in biofilm systems. Liu et al. (27) described an observed growth yield in biofilms that takes channeling of dissolved organic carbon to CO_2 and biomass fractions into account. According to the equation presented by these authors for the observed growth yield it is clear that, given a finite dissolved organic carbon source, an increase in respiration will imply a decrease in biomass as the authors indeed show with data from the literature.

It has been proposed that under conditions of energy limitation, catabolic reactions are tightly coupled to anabolic reactions (41) and diversion of substrate carbon into extracellular products is minimized (14). Our studies show that between 40% and 50% of the inflowing carbon is used for respiration; ~25% exits during the gas phase, and a similar amount remains dissolved and exits during the liquid phase. Furthermore, around 30% of the carbon leaves as dense aggregates, presumably consisting of cells bound to the EPS. Even if cell density in the aggregates is assumed to be similar to values of the biofilm, it means that roughly 20% of the carbon is converted to EPS and released to the effluent, even though our system may be considered carbon limited (Beyenal et al. [4] considered 5 mM of glucose to be a carbon-limiting condition in *P. aeruginosa* chemostat cultures). Our focus here is not to elucidate the different EPS fractions; for that, refer to the seminal work by Laspidou and Rittmann (22) who discussed EPS and soluble microbial products with their various subfractions and address the confusion regarding terminology that originated because EPSs have historically been studied from various backgrounds. In brief, a common theme of EPSs (bound and soluble) and soluble microbial products is that they are both organic materials of microbial origins but do not contain any active cells. These authors also reported EPS values as a percentage of influent carbon for continuously stirred tank and batch reactors.

Our data suggest that the measurement of CO_2 in the off-gas is a suitable way of determining biofilm metabolic responses to changes in environmental parameters given the linear relationship to dissolved CO_2 under the conditions used. For changes in citrate concentration, the metabolic responses of *Pseudomonas* sp. strain CT07 *gfp* and *P. aeruginosa* PA01 *gfp* were nearly linear for values above 0.5 mM, which would suggest a regime of carbon sufficiency for those particular biofilms. For values below 0.5 mM citrate, the response deviated from linearity and can be explained in terms of a threshold level of nutrients required for maintenance. When the level of available substrate carbon is lower than the value required for maintenance, the microbial cell must use carbon from its reserves (52).

The biofilm metabolic response was sensitive even to small changes in temperature. It should be noted that for the measurement of the temperature response, neither the silicone permeability dependence on temperature nor the temperature influence on gas solubility was taken into account. The gas permeability of silicone increases with increasing temperatures according to an Arrhenius-type relationship (36), while the solubility of CO_2 in growth media increases with decreasing temperatures. However, these influences should be negligible over the temperature ranges used in these experiments.

With equation 6, the overall transfer coefficient for the CEMS, K_L, can be determined for known dissolved CO_2 concentrations by measuring the CO_2 flux in the off-gas. We have not yet determined the K_L because of the requirement of the constant dissolved CO_2 concentration, C_1, in the derivation of equation 6. The requirement for constant C_1 could be accomplished by either increasing the dissolved CO_2 concentration and assuming that the CO_2 loss across the membrane is neg-

ligible or by shortening the length of the CEMS to minimize the loss of CO_2 along the length of the silicone tube. Once the K_L has been determined, the resulting equation shows a linear relationship between the dissolved CO_2 and the CO_2 measured in the gas phase. Frahm et al. (10) simultaneously solved a set of differential equations to relate carbon dioxide transfer rate measurements (measured in the gas phase) in mammalian suspension cultures to the carbon dioxide production rate. The equations included information about pH changes, buffer, and media composition and CO_2 transfer from the liquid phase to the gas phase. Weissenbacher et al. (55) used a similar approach to calculate the carbon dioxide production rate from the carbon dioxide transfer rate measurements in activated sludge systems by correcting for the dissolved CO_2/bicarbonate equilibrium transformations. Although our method is slightly less sophisticated by considering only a clumped transfer coefficient, it seems that we are still able to predictably relate dissolved CO_2 with CO_2 measured in the gas phase.

In systems considering mass transfer from the gas-to-liquid phase via membranes, liquid and gas flow rates influence the transfer rate. Zhang et al. (61) determined that in the case of physical absorption (when CO_2 does not react with liquid it dissolves into water, and the authors considered CO_2 dissolving into water as a physical process), the CO_2 flux across the membrane increased with liquid velocity while the gas velocity had no effect on the CO_2 flux when the direction of transfer was from gas to liquid. A reason for increased transfer would be an increase in the gradient of the driving force across the membrane. In our system, the liquid phase concentration is assumed to be constant but an increase in the gas flow rate will result in a lower average CO_2 concentration on the gas side, which will increase the driving force gradient for an increased transfer rate. Caution is therefore necessary to ensure constant gas flow rates while using the CEMS during the same experiment.

In conclusion, the CEMS proved to be a useful tool for nondestructive, real-time monitoring of biofilm metabolic activity. Using this approach, it was shown that biofilms responded rapidly to changes in nutrients and temperature. The nondestructive nature of this approach renders it appropriate to accurately and rapidly assess the influence of other environmental conditions on overall biofilm activity, including antimicrobials, nutrient limitation, and microbial community interactions such as predation, competition for a finite substrate, or cooperation to utilize recalcitrant molecules. This approach should therefore not be limited to pure cultures and defined laboratory media; it also provides a measured parameter (CO_2 production as a measure of biofilm activity) with a potential application in mathematical models. In the current research, the CEMS made it possible to determine carbon channeling by biofilm cells, showing that a small fraction (<5%) of the influent carbon is retained in the biofilm, which is a relatively small investment, enabling the biofilm to serve as a catalytic unit to transform carbon from the surrounding environment.

ACKNOWLEDGMENTS

Financial support was provided by the Canada Research Chair Program, NSERC (G.M.W.), and a Ryerson Graduate Award (O.K.).

We thank Leandro Boonzaaier for assistance in the derivation of the transfer equations.

REFERENCES

1. **Aboka, F. O., H. Yang, L. P. De Jonge, R. Kerste, W. A. Van Winden, W. M. Van Gulik, R. Hoogendijk, A. Oudshoorn, and J. J. Heijnen.** 2006. Characterization of an experimental miniature bioreactor for cellular perturbation studies. Biotechnol. Bioeng. **95:**1032–1042.
2. **Anonymous.** 2005. ASTM standard F 2476-05, standard test method for the determination of carbon dioxide gas transmission rate (CO_2TR) through barrier materials using an infrared detector. ASTM International, West Conshohocken, PA.
3. **Bester, E., G. Wolfaardt, L. Joubert, K. Garny, and S. Saftic.** 2005. Planktonic-cell yield of a pseudomonad biofilm. Appl. Environ. Microbiol. **71:** 7792–7798.
4. **Beyenal, H., S. N. Chen, and Z. Lewandowski.** 2003. The double substrate growth kinetics of *Pseudomonas aeruginosa*. Enzyme Microb. Technol. **32:** 92–98.
5. **Côté, P., J.-L. Bersillon, and A. Huyard.** 1989. Bubble-free aeration using membranes: mass transfer analysis. J. Membr. Sci. **47:**91–106.
6. **Dahod, S. K.** 1993. Dissolved carbon dioxide measurement and its correlation with operating parameters in fermentation processes. Biotechnol. Prog. **9:**655–660.
7. **Delille, A., F. Quilés, and F. Humbert.** 2007. In situ monitoring of the nascent *Pseudomonas fluorescens* biofilm response to variations in the dissolved organic carbon level in low-nutrient water by attenuated total reflectance-Fourier transform infrared spectroscopy. Appl. Environ. Microbiol. **73:**5782–5788.
8. **Dindore, V. Y., D. W. F. Brilman, P. H. M. Feron, and G. F. Versteeg.** 2004. CO_2 absorption at elevated pressures using a hollow fiber membrane contactor. J. Membr. Sci. **235:**99–109.
9. **Flemming, H.-C.** 2003. Role and levels of real-time monitoring for successful anti-fouling strategies—an overview. Water Sci. Technol. **47**(5)**:**1–8.
10. **Frahm, B., H.-C. Blank, P. Cornand, W. Oelßner, U. Guth, P. Lane, A. Munack, K. Johannsen, and R. Portner.** 2002. Determination of dissolved CO_2 concentration and CO_2 production rate of mammalian cell suspension culture based on off-gas measurement. J. Biotechnol. **99:**133–148.
11. **Geesey, G. G., R. Mutch, J. W. Costerton, and R. B. Green.** 1978. Sessile bacteria: an important component of the microbial population in small mountain streams. Limnol. Oceanogr. **23:**1214–1223.
12. **Gillooly, J. F., J. H. Brown, G. B. West, V. M. Savage, and E. L. Charnov.** 2001. Effects of size and temperature on metabolic rate. Science **293:**2248–2251.
13. **Haisch, C., and R. Niessner.** 2007. Visualisation of transient processes in biofilms by optical coherence tomography. Water Res. **41:**2467–2472.
14. **Harder, W., and L. Dijkhuizen.** 1983. Physiological responses to nutrient limitation. Annu. Rev. Microbiol. **37:**1–23.
15. **Hoffman, E. J.** 2003. Membrane separations technology: single-stage, multistage, and differential permeation. Gulf Professional Publishing, Amsterdam, The Netherlands.
16. **Janknecht, P., and L. F. Melo.** 2003. Online biofilm monitoring. Rev. Environ. Sci. Biotechnol. **2:**269–283.
17. **Jenkins, D. M., and A. Krishnan.** 2004. Surface limitations for gas transport through a silicone film, p. 3973–3984. American Society of Agricultural and Biological Engineers, St. Joseph, MI.
18. **Jones, R. P., and P. F. Greenfield.** 1982. Effect of carbon dioxide on yeast growth and fermentation. Enzyme Microb. Technol. **4:**210–223.
19. **Kappelhof, J. W. N. M., H. S. Vrouwenvelder, M. Schaap, J. C. Kruithof, D. Van Der Kooij, and J. C. Schippers.** 2003. An in situ biofouling monitor for membrane systems. Water Sci. Technol. **3**(5)**:**205–210.
20. **Klahre, J., and H.-C. Flemming.** 2000. Monitoring of biofouling in papermill process waters. Water Res. **34:**3657–3665.
21. **Kreft, J.-U.** 2004. Biofilms promote altruism. Microbiology **150:**2751–2760.
22. **Laspidou, C. S., and B. E. Rittmann.** 2002. A unified theory for extracellular polymeric substances, soluble microbial products, and active and inert biomass. Water Res. **36:**2711–2720.
23. **Lawrence, J. R., D. R. Korber, G. M. Wolfaardt, and D. E. Caldwell.** 1995. Behavioural strategies of surface colonizing bacteria. Adv. Microb. Ecol. **14:**1–75.
24. **Lee, H. J., D. G. Han, S. H. Lee, J. W. Yoo, S. H. Baek, and E. K. Lee.** 1998. On-line monitoring and quantitative analysis of biofouling in low-velocity cooling water system. Korean J. Chem. Eng. **15:**71–77.
25. **Lee, J.-H., Y. Seo, T.-S. Lim, P. L. Bishop, and I. Papautsky.** 2007. MEMS needle-type sensor array for in situ measurements of dissolved oxygen and redox potential. Environ. Sci. Technol. **41:**7857–7863.
26. **Lewandowski, Z., and H. Beyenal.** 2003. Biofilm monitoring: a perfect solution in search of a problem. Water Sci. Technol. **47**(5)**:**9–18.
27. **Liu, Y., Y.-M. Lin, S.-F. Yang, and J.-H. Tay.** 2003. A balanced model for biofilms developed at different growth and detachment forces. Process Biochem. **38:**1761–1765.
28. **Ludensky, M. L.** 1998. An automated system for biocide testing on biofilms. J. Ind. Microbiol. Biotechnol. **20:**109–115.
29. **Marshall, K. C., R. Stout, and R. Mitchell.** 1971. Selective sorption of bacteria from seawater. Can. J. Microbiol. **17:**1413–1416.

30. **Massana, R., J. M. Gasol, P. K. Bjørnsen, N. Blackburn, A. Hagstrom, S. Hietanen, B. H. Hygum, J. Kuparinen, and C. Pedrós-Alió.** 1997. Measurement of bacterial size via image analysis of epifluorescence preparations: description of an inexpensive system and solutions to some of the most common problems. Sci. Mar. **61:**397–407.
31. **Maurício, R., C. J. Dias, and F. Santana.** 2006. Monitoring biofilm thickness using a non-destructive, on-line, electrical capacitance technique. Environ. Monit. Assess. **119:**599–607.
32. **Mavroudi, M., S. P. Kaldis, and G. P. Sakellaropoulos.** 2006. A study of mass transfer resistance in membrane gas-liquid contacting processes. J. Membr. Sci. **272:**103–115.
33. **Milferstedt, K., M.-N. Pons, and E. Morgenroth.** 2006. Optical method for long-term and large-scale monitoring of spatial biofilm development. Biotechnol. Bioeng. **94:**773–782.
34. **Mollica, A., and P. Cristiani.** 2003. On-line biofilm monitoring by "BIOX" electrochemical probe. Water Sci. Technol. **47**(5)**:**45–49.
35. **Mueller, R. F.** 1996. Bacterial transport and colonization in low nutrient environments. Water Res. **30:**2681–2690.
36. **Mulder, M.** 1996. Basic principles of membrane technology. Kluwer Academic, Dordrecht, The Netherlands.
37. **Pietikäinen, J., M. Pettersson, and E. Baath.** 2005. Comparison of temperature effects on soil respiration and bacterial and fungal growth rates. FEMS Microbiol. Ecol. **52:**49–58.
38. **Posch, T., M. Loferer-Kroßbacher, G. Gao, A. Alfreider, J. Pernthaler, and R. Psenner.** 2001. Precision of bacterioplankton biomass determination: a comparison of two fluorescent dyes, and of allometric and linear volume-to-carbon conversion factors. Aquat. Microb. Ecol. **25:**55–63.
39. **Richter, L., C. Stepper, A. Mak, A. Reinthaler, R. Heer, M. Kast, H. Bruckl, and P. Ertl.** 2007. Development of a microfluidic biochip for online monitoring of fungal biofilm dynamics. Lab. Chip **7:**1723–1731.
40. **Robb, W. L.** 1968. Thin silicone membranes—their permeation properties and some applications. Ann. N. Y. Acad. Sci. **146:**119–137.
41. **Russell, J. B., and G. M. Cook.** 1995. Energetics of bacterial growth: balance of anabolic and catabolic reactions. Microbiol. Rev. **59:**48–62.
42. **Sauer, K., A. K. Camper, G. D. Ehrlich, J. W. Costerton, and D. G. Davies.** 2002. *Pseudomonas aeruginosa* displays multiple phenotypes during development as a biofilm. J. Bacteriol. **184:**1140–1154.
43. **Schmid, T., U. Panne, J. Adams, and R. Niessner.** 2004. Investigation of biocide efficacy by photoacoustic biofilm monitoring. Water Res. **38:**1189–1196.
44. **Seymour, J. D., S. L. Codd, E. L. Gjersing, and P. S. Stewart.** 2004. Magnetic resonance microscopy of biofilm structure and impact on transport in a capillary bioreactor. J. Magn. Reson. **167:**322–327.
45. **Sirkar, K. K.** 1992. Other new membrane processes, p. 885–912. *In* W. S. W. Ho and K. K. Sirkar (ed.), Membrane handbook. Van Nostrand Reinhold, New York, NY.
46. **Spaeth, E. E., and S. K. Friedlander.** 1967. The diffusion of oxygen, carbon dioxide, and inert gas in flowing blood. Biophys. J. **7:**827–851.
47. **Stoodley, P., K. Sauer, D. G. Davies, and J. W. Costerton.** 2002. Biofilms as complex differentiated communities. Annu. Rev. Microbiol. **56:**187–209.
48. **Tam, K., N. Kinsinger, P. Ayala, F. Qi, W. Shi, and N. V. Myung.** 2007. Real-time monitoring of *Streptococcus mutans* biofilm formation using a quartz crystal microbalance. Caries Res. **41:**474–483.
49. **Tamachkiarow, A., and H.-C. Flemming.** 2003. On-line monitoring of biofilm formation in a brewery water pipeline system with a fibre optical device. Water Sci. Technol. **47**(5)**:**19–24.
50. **Tanji, Y., T. Nishihara, and K. Miyanaga.** 2007. Monitoring of biofilm in cooling water system by measuring lactic acid consumption rate. Biochem. Eng. J. **35:**81–86.
51. **Teixeira de Mattos, M. J., and O. M. Neijssel.** 1997. Bioenergetic consequences of microbial adaptation to low-nutrient environments. J. Biotechnol. **59:**117–126.
52. **Touratier, F., L. Legendre, and A. Vézina.** 1999. Model of bacterial growth influenced by substrate C:N ratio and concentration. Aquat. Microb. Ecol. **19:**105–118.
53. **Vanhooren, H., D. Demey, I. Vannijvel, and P. A. Vanrolleghem.** 2000. Monitoring and modelling an industrial trickling filter using on-line off-gas analysis and respirometry. Water Sci. Technol. **41**(12)**:**139–148.
54. **Visser, D., G. A. Van Zuylen, J. C. Van Dam, A. Oudshoorn, M. R. Eman, C. Ras, W. M. Van Gulik, J. Frank, G. W. K. Van Dedem, and J. J. Heijnen.** 2002. Rapid sampling for analysis of in vivo kinetics using the BioScope: a system for continuous-pulse experiments. Biotechnol. Bioeng. **79:**674–681.
55. **Weissenbacher, N., K. Lenz, S. N. Mahnik, B. Wett, and M. Fuerhacker.** 2007. Determination of activated sludge biological activity using model corrected CO_2 off-gas data. Water Res. **41:**1587–1595.
56. **Wolf, G., J. G. Crespo, and M. A. M. Reis.** 2002. Optical and spectroscopic methods for biofilm examination and monitoring. Rev. Environ. Sci. Biotechnol. **1:**227–251.
57. **Xavier, J. B., and K. R. Foster.** 2007. Cooperation and conflict in microbial biofilms. Proc. Natl. Acad. Sci. USA **104:**876–881.
58. **Yasuda, H.** 1975. Units of gas permeability constants. J. Appl. Polym. Sci. **19:**2529–2536.
59. **Zeng, A.-P.** 1995. Effect of CO_2 absorption on the measurement of CO_2 evolution rate in aerobic and anaerobic continuous cultures. Appl. Microbiol. Biotechnol. **42:**688–691.
60. **Zhang, H.-Y., R. Wang, D. T. Liang, and J. H. Tay.** 2008. Theoretical and experimental studies of membrane wetting in the membrane gas-liquid contacting process for CO_2 absorption. J. Membr. Sci. **308:**162–170.
61. **Zhang, H.-Y., R. Wang, D. T. Liang, and J. H. Tay.** 2006. Modeling and experimental study of CO_2 absorption in a hollow fiber membrane contactor. J. Membr. Sci. **279:**301–310.